

Communication

Substituted Azolium Disposition: Examining the Effects of Alkyl Placement on Thermal Properties

Karel Goossens ^{1,*},[†] , Lena Rakers ^{2,†}, Tae Joo Shin ³, Roman Honeker ²,
Christopher W. Bielawski ^{1,4,5,*}  and Frank Glorius ^{2,*} 

¹ Center for Multidimensional Carbon Materials (CMCM), Institute for Basic Science (IBS), Ulsan 44919, Korea

² Organisch-Chemisches Institut, Westfälische Wilhelms-Universität Münster, Corrensstraße 40, 48149 Münster, Germany; lena.roling@uni-muenster.de (L.R.); honeker@gmx.de (R.H.)

³ UNIST Central Research Facilities (UCRF) and School of Natural Science, Ulsan National Institute of Science and Technology (UNIST), Ulsan 44919, Korea; tjshin@unist.ac.kr

⁴ Department of Chemistry, UNIST, Ulsan 44919, Korea

⁵ Department of Energy Engineering, UNIST, Ulsan 44919, Korea

* Correspondence: karel.cw.goossens@gmail.com (K.G.); bielawski@unist.ac.kr (C.W.B.); glorius@uni-muenster.de (F.G.); Tel.: +82-52-217-2952 (C.W.B.); +49-251-8333248 (F.G.)

† These authors contributed equally to this work.

Received: 23 December 2018; Accepted: 6 January 2019; Published: 11 January 2019



Abstract: We describe the thermal phase characteristics of a series of 4,5-bis(*n*-alkyl)azolium salts that were studied using thermogravimetric analysis (TGA), differential scanning calorimetry (DSC), polarized-light optical microscopy (POM), and synchrotron-based small- to wide-angle X-ray scattering (SWAXS) measurements. Key results were obtained for 1,3-dimethyl-4,5-bis(*n*-undecyl)imidazolium iodide (**1-11**), 1,3-dimethyl-4,5-bis(*n*-pentadecyl)imidazolium iodide (**1-15**), and 1,2,3-trimethyl-4,5-bis(*n*-pentadecyl)imidazolium iodide (**2**), which were found to adopt enantiotropic smectic A mesophases. Liquid-crystalline mesophases were not observed for 1,3-dimethyl-4,5-bis(*n*-heptyl)imidazolium iodide (**1-7**), 3-methyl-4,5-bis(*n*-pentadecyl)thiazolium iodide (**3**), and 2-amino-4,5-bis(*n*-pentadecyl)imidazolium chloride (**4**). Installing substituents in the 4- and 5-positions of the imidazolium salts appears to increase melting points while lowering clearing points when compared to data reported for 1,3-disubstituted analogues.

Keywords: liquid crystals; ionic liquid crystals; ionic liquids; imidazolium; thiazolium; mesophases

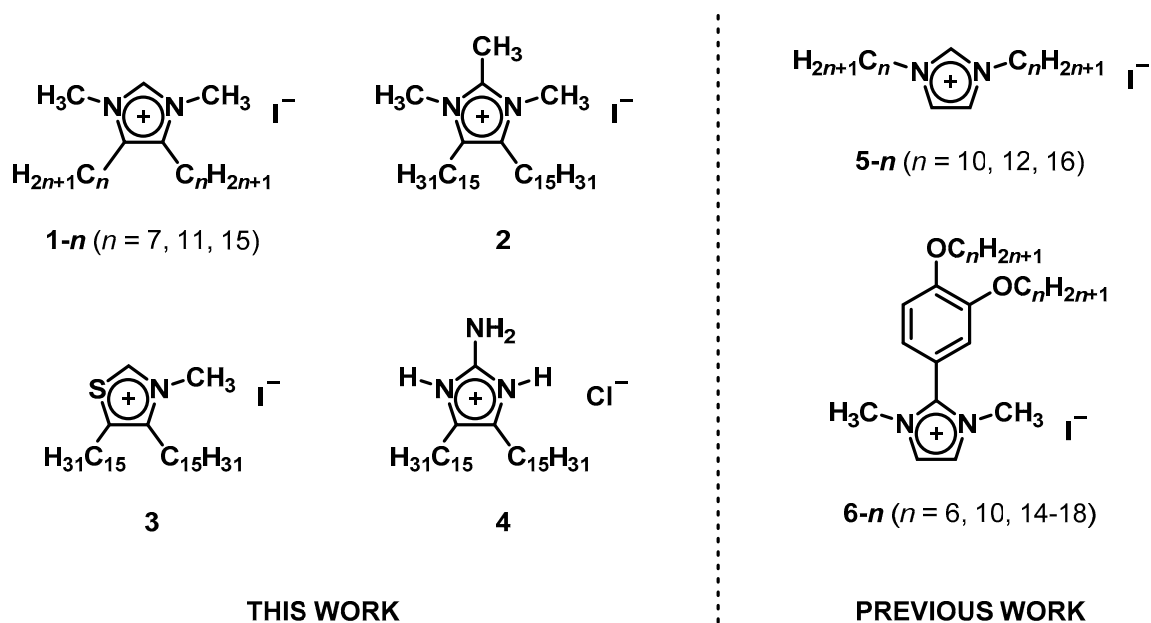
1. Introduction

Attachment of relatively long alkyl or fluoroalkyl chains to the nitrogen atoms of heterocyclic cations, such as imidazolium moieties, typically bestows thermotropic liquid-crystalline (LC) properties due to an enhancement in amphiphilicity [1–4]. Ionic liquid crystals (ILCs) are of high interest because they hold potential for use in a variety of applications [5–9]. For instance, it has already been demonstrated that ILCs may be used as non-volatile electrolytes in dye-sensitized solar cells [10–12], as organized reaction media [13], and as active components in electrochromic devices that do not require additional electrolytes [14–16]. On a more fundamental level, a comprehensive knowledge of the structural parameters that determine the thermal properties of ILCs and the long-range supramolecular organization in their mesophases contributes to a better understanding of the short-range nanosegregation phenomena that occur in room-temperature ionic liquids (ILs) [17–27]. Such structure–property relationships may also improve molecular designs of new ILCs and ILs, and facilitate tailoring for specific applications.

Although imidazolium moieties are among the most widely used cationic cores to obtain ILCs, the majority of studies have focused on *N*-substituted derivatives due to the ease of their synthesis [5–7,28–30].

The influence of installing alkyl or aryl substituents in the 2-position of imidazolium-based ILCs on thermal phase characteristics has also been investigated [31–40]. To the best of our knowledge, only one LC imidazolium salt with a substituent in the 4-position, 1,3,4-trimethylimidazolium *n*-dodecylsulfonate, is known and was reported to adopt a monotropic smectic A (SmA) phase ($\text{Cr} \cdot (\text{SmA} \cdot 93 \cdot) 95 \cdot \text{Iso} (\text{°C})$) [32]. For comparison, 1,3-dimethylimidazolium *n*-dodecylsulfonate self-organizes into an enantiotropic SmA phase upon heating and displays a considerably higher clearing point ($\text{Cr} \cdot 90 \cdot \text{SmA} \cdot 177 \cdot \text{Iso} (\text{°C})$) whereas the corresponding 1,2,3-trimethylimidazolium ($\text{Cr} \cdot 202 \cdot \text{Iso} (\text{°C})$) and 1,3,4,5-tetramethylimidazolium ($\text{Cr} \cdot 109 \cdot \text{Iso} (\text{°C})$) salts are not LC [32]. Even in the realm of ILCs, limited physical property data are available for tri-, tetra-, and pentasubstituted imidazolium salts (with the additional substituents often being limited to methyl groups) [29,30,41–48]. Beyond differences in thermal properties, highly substituted imidazolium salts may be expected to show an increased stability toward base, particularly if they are to be used in, for instance, alkaline fuel cell membranes [49].

Recently, some of us prepared a series of 4,5-bis(*n*-alkyl)imidazolium salts by utilizing Radziszewski-type chemistry for the formation of the requisite heterocyclic cores [50–53]. In addition, 4,5-bis(*n*-pentadecyl)thiazolium salts were synthesized from a thiazole precursor that was obtained by reacting P_2S_5 , formamide and 17-bromodotriacontan-16-one [51]. The bromoketone was also used to prepare a novel guanidinium salt (i.e., 4,5-bis(*n*-pentadecyl)imidazolium with an amino group in the 2-position) [51]. The aforementioned salts were studied as lipid analogues in model cell systems or used as precursors for *N*-heterocyclic carbenes for the stabilization of nanoparticles [50–53]. From the library of compounds, we selected six 4,5-bis(*n*-alkyl)azolium salts (**1–*n*** ($n = 7, 11, 15$) and **2–4**, Scheme 1) and investigated their thermal characteristics. The data were compared with those reported for analogous 1,3-bis(*n*-alkyl)imidazolium and 2-[3,4-bis(*n*-alkoxy)phenyl]-1,3-dimethylimidazolium ILCs (for example, **5–*n*** and **6–*n*** in Scheme 1) [38,54–59]. Collectively, the results that will be described below show how the disposition of long alkyl chains around five-membered, heteroaromatic, cationic cores affects the thermal characteristics of the resulting salts.



Scheme 1. Left: overview of the 4,5-bis(*n*-alkyl)azolium salts that were investigated in this work. Right: previously reported imidazolium salts that feature two relatively long alkyl chains [38,54].

2. Materials and Methods

The synthesis of compounds **1–*n*** and **2–4** has been described elsewhere [50,51].

Optical textures were observed using an Olympus BX53-P polarized-light optical microscope that was equipped with a rotatable graduated sample platform and an Instec HCS402 dual heater

temperature stage. The latter was equipped with a precision XY positioner, and was coupled to an Instec LN₂-SYS liquid nitrogen cooling system and an Instec mK2000 programmable temperature controller. Images were recorded by a QImaging Retiga 2000R CCD camera that was coupled to the microscope. The samples were pressed between an untreated glass slide and glass coverslip (0.13–0.17 mm thick, Duran) prior to analysis.

Differential scanning calorimetry (DSC) data were recorded under nitrogen (50 mL·min⁻¹) on a TA Instruments DSC Q2000 module equipped with an RCS90 cooling system at a heating rate of 10 °C·min⁻¹ and a cooling rate of 5 °C·min⁻¹. The quantity of sample analyzed was typically 4–5 mg. A small hole was pierced into the lid of the aluminum sample pans. The measurements were performed using the Tzero™ Heat Flow T4P option. High-purity sapphire disks were used for the Tzero™ calibration and high-purity indium was used as a standard for temperature and enthalpy calibrations. DSC data analysis was performed with the Universal Analysis 2000 software (version 4.5A) from TA Instruments (New Castle, DE, USA). The abbreviations used to describe the thermal phase properties are explained in the main text and in the captions of the figures and tables.

Thermogravimetric analysis (TGA) data were recorded under nitrogen (60 mL·min⁻¹) on a TA Instruments TGA Q500 module at a heating rate of 5 °C·min⁻¹ and using a platinum sample pan. The quantity of sample analyzed was typically 5–8 mg. High-purity nickel was used as a standard for temperature calibration (based on its Curie temperature).

Synchrotron-based X-ray scattering measurements were performed at the PLS-II 6D UNIST-PAL Beamline of the Pohang Accelerator Laboratory (PAL), Pohang, Republic of Korea. The X-rays coming from the bending magnet were monochromated using Si(111) double crystals and focused at the detector position by the combination of a second, sagittal-type monochromator crystal and a toroidal mirror system. The diffraction patterns were recorded by a Rayonix MX225-HS 2D CCD detector (225 × 225 mm² square active area, full resolution 5760 × 5760 pixels) with 2 × 2 binning. The peak positions in the 1D intensity profiles, which were obtained from azimuthal averaging of the 2D patterns of non-aligned samples (with dezingering applied to the data of two separate measurements), were used for phase type assignments. Small- to wide-angle X-ray scattering (SWAXS) patterns (for periodicities up to 67 Å) were recorded using 12.3984 keV X-ray radiation (wavelength $\lambda = 1.00$ Å) and a sample-to-detector distance (SDD) of ca. 431 mm. Diffraction angles were calibrated using a lanthanum hexaboride (LaB₆) standard (NIST SRM 660c). Samples were contained in borosilicate glass (glass #50) capillaries with an outer diameter of 0.4 mm and a wall thickness of 10 μ m and were irradiated for 10–30 s per measurement, depending on the saturation level of the detector. The capillaries were inserted into a custom-made brass holder that was placed into a Linkam TS1500V heating stage to achieve temperature control. The samples were allowed to equilibrate at each temperature before starting a measurement.

Molecular models were created using the Chem3D Pro 15.1 software package (PerkinElmer Informatics, Inc., Waltham, MA, USA).

3. Results

We examined the thermal properties of 4,5-bis(*n*-alkyl)azolium salts **1-*n*** and **2-4** using TGA, DSC, and polarized-light optical microscopy (POM). Key results are summarized in Table 1. Figures showing the TGA and DSC thermograms can be found in the Supplementary Material (Figures S1–S7).

Table 1. Summary of phase transition temperatures and other thermal data recorded for the 4,5-bis(*n*-alkyl)azolium salts **1-*n*** (*n* = 7, 11, 15) and **2-4**, as well as corresponding assignments.

Compound	Transition ¹	<i>T</i> (°C) ²	ΔH (kJ·mol ⁻¹) ³	<i>T</i> _{1%} (°C) ⁴
1-7	Cr → Iso ⁵	26	0.7	n.d.
1-11	HR1: Cr → SmA ⁶	50, 55 ⁶	21.6 ⁶	n.d.
	SmA → Iso	77	2.3	
1-15	HR2: g → SmA	~−14	−	
	SmA → Iso	76	2.2	
	Cr → SmA	76	38.3	~181
2	SmA → Iso	88 ⁷	0.7	
	Cr → SmA ⁸	70 ⁸	− ⁸	~194
3	SmA → Iso	88 ⁷	0.5	
	Cr → Iso ⁹	73 ⁷	16.4	~135
4	Cr → Iso ⁹	68 ⁷	38.1	~206

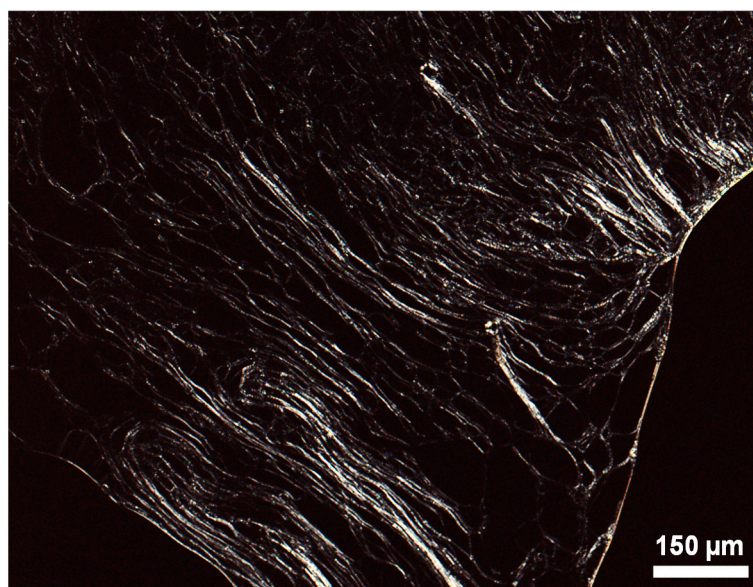
¹ Abbreviations: Cr = crystalline phase; g = glass; SmA = smectic A phase; Iso = isotropic liquid phase. HR1 = first heating run; HR2 = second heating run. ² Onset temperatures obtained by DSC during the second heating run (unless indicated otherwise) at a rate of 10 °C·min⁻¹ and under an atmosphere of N₂ (50 mL·min⁻¹). A small hole was pierced into the lid of the DSC sample pans. The glass transition temperature was defined by the inflection point of the signal recorded in the respective DSC thermogram. ³ Enthalpy change. ⁴ Temperature at which 1% weight loss was measured by TGA (neglecting initial small weight losses attributed to the release of H₂O). n.d. = not determined. ⁵ During the second heating run, melting was preceded by an exothermic recrystallization event with a peak temperature of 22 °C ($\Delta H = -0.4$ kJ·mol⁻¹) (Figure S1). ⁶ This transition involved two, partially resolved transitions between 37 °C and 68 °C (Figure S2). The peak temperatures of the two signals and the total enthalpy change are listed. Examination by POM revealed that the sample became plastic after the first transition upon heating. ⁷ Peak temperature. ⁸ The transition to the LC mesophase upon heating was preceded by multiple transitions (Figure S4). The peak temperature of the last endothermic signal just before the temperature range of the SmA phase is given. Examination by POM revealed that the sample gradually became plastic above ~50 °C upon heating. The enthalpy change associated with the transition from the SmA phase to the solid state at 40 °C upon cooling was measured to be 12.2 kJ·mol⁻¹. ⁹ Melting was preceded by solid-to-solid transitions (Figures S5 and S6).

The slightly higher thermal stability measured for **2** as compared to salt **1-15** can be ascribed to the replacement of the acidic H(2) proton of the imidazolium with a methyl group. The result is in accordance with the generally observed higher thermal stabilities of 2-methylsubstituted 1,3-dialkylimidazolium ILs relative to their unsubstituted counterparts [60]. The 3,4,5-trialkylsubstituted thiazolium salt **3** showed a relatively low thermal stability, with weight losses starting to occur at about 135 °C under the conditions employed for the TGA measurements. The most thermally stable salt among the compounds that were studied was **4** (*T*_{1%} ≈ 206 °C), despite the fact that it contains nucleophilic Cl⁻ anions as well as amino groups.

DSC and POM investigations of compounds **1-*n*** and **2-4** led to the conclusion that imidazoliums **1-11**, **1-15**, and **2** are thermotropic ILCs but imidazolium **1-7**, thiazolium **3**, and guanidinium **4** are not. To the best of our knowledge, **2** is the first example of a LC pentasubstituted imidazolium salt. Salt **1-7**, which was obtained as a partially crystallized compound, melted to an isotropic liquid around room temperature. In contrast, solid samples of **1-11**, **1-15**, and **2**, which are more amphiphilic than **1-7**, melted to birefringent mesophases which produced “oily streaks” when viewed by POM (Figure 1). Homeotropic domains were observed as well. Further heating facilitated transitions to isotropic liquid states, for which, in the case of **1-15** and **2**, only weak signals were observed in the DSC thermograms (Figure 2 and Figures S2–S4). Upon cooling, ill-shaped “bâtonnets” were seen by POM upon entering the LC states and gradually transformed into focal-conic-like textures with further cooling. In the case of **1-11**, the sample spontaneously aligned homeotropically when cooled from the isotropic liquid state and the LC mesophase vitrified around −23 °C; glass transitions continued to be seen during subsequent heating/cooling cycles (Figure 2a). The non-mesomorphic salts **3** and **4** melted directly to isotropic liquids without passing through intermediate LC phases. The melting point data recorded for all 4,5-bis(*n*-pentadecyl)azolium salts (**1-15** and **2-4**) are similar and situated in the range of 68 to 76 °C.



(a)



(b)

Figure 1. Polarized-light optical microscopy (POM) images of the SmA phases of (a) **1-11** at 24 °C (upon cooling from the isotropic liquid state and after applying pressure to the sample) and (b) **2** at 77 °C (during the first heating run of a pristine sample).

Synchrotron-based small- to wide-angle X-ray scattering (SWAXS) measurements of the LC mesophases adopted by **1-15** and **2** afforded patterns that were characterized by two sharp reflections in the small-angle region, in addition to a diffuse wide-angle scattering signal centered at 4.4–4.6 Å (Figure 3, Table 2 and Figure S8). The latter corresponds to the lateral short-range order of the molten alkyl chains (c.f. h_{ch}) and the ionic headgroups (c.f. h_{ion}), respectively, which were not resolved in the experimental data. The reciprocal d -spacings of the sharp small-angle reflections were related by a 1:2 ratio and the signals can be indexed as the (001) and (002) reflections that originate from the formation of layers. Collectively, the POM and SWAXS data indicate that the LC mesophases adopted by salts **1-15** and **2** are SmA phases. A slightly larger layer thickness was found for **2** as compared with **1-15** at similar temperatures (see Table 2), which can be ascribed to the protruding 2-methyl substituents in the former. Based on the POM observations, the mesophase adopted by **1-11** is also a SmA phase.

SWAXS patterns that were recorded for **3** at different temperatures revealed that the sample adopted a lamellar structure in the solid state before melting to an isotropic liquid at about 73 °C (Figure S9).

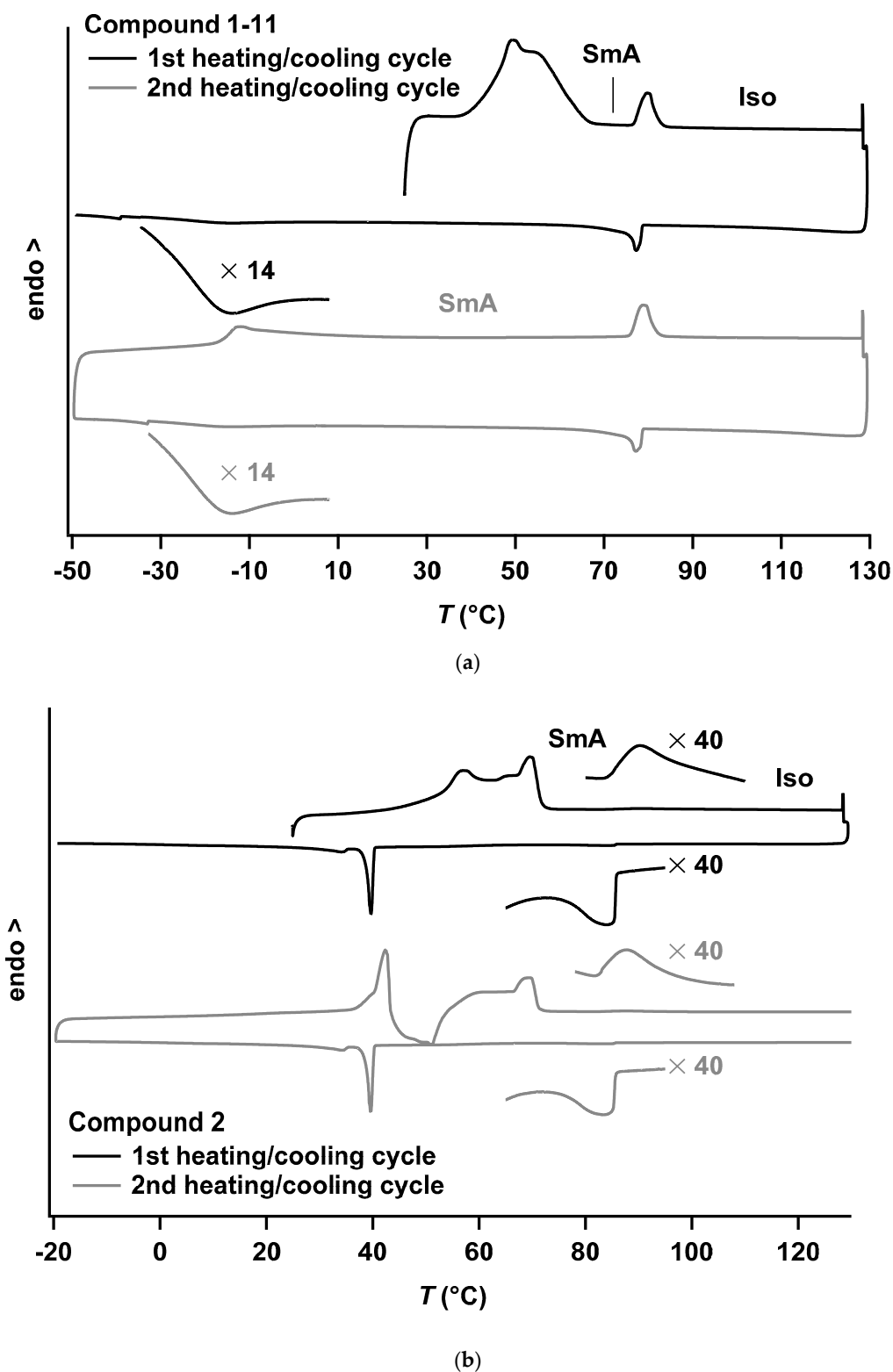


Figure 2. Differential scanning calorimetry (DSC) data recorded for (a) **1-11** and (b) **2** at a heating rate of 10 °C·min⁻¹ and a cooling rate of 5 °C min⁻¹ under an atmosphere of N₂. Endothermic peaks point upward.

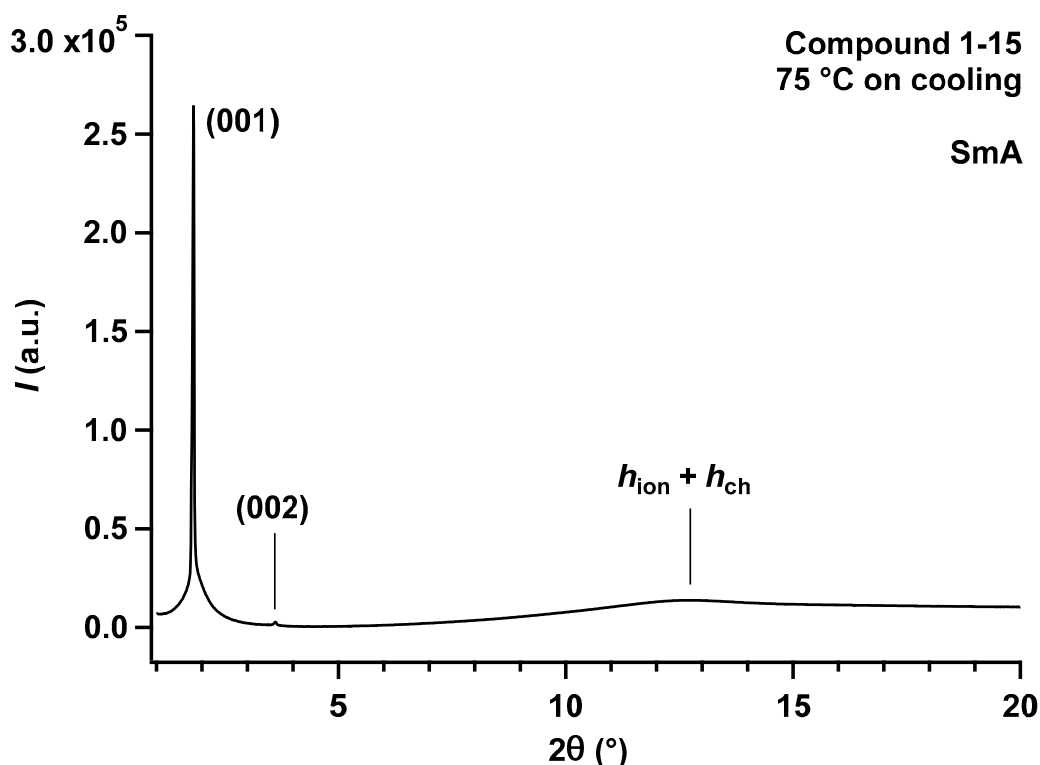


Figure 3. Synchrotron-based SWAXS data that were recorded for the SmA phase of **1-15** at 75 °C upon cooling (the X-ray wavelength used was 1.00 Å).

Table 2. Summary of synchrotron-based SWAXS data recorded for the LC mesophases adopted by **1-15** and **2**, including calculated structural parameters and corresponding assignments.

Cpd.	Type of LC Mesophase	<i>T</i> (°C)	<i>d</i> _{obs.} (Å) ¹	<i>I</i> ²	<i>hkl</i> ³	<i>d</i> _{calcd.} (Å) ¹	Structural Parameters of the LC Mesophases ⁴
1-15	SmA	75 (upon cooling)	31.63	VS (sh)	001	31.68	<i>d</i> = 31.68 Å <i>V</i> _{mol} ≈ 1072 Å ³ <i>A</i> _M ≈ 67.7 Å ² <i>σ</i> _{ch} ≈ 22.1 Å ²
			15.86	W (sh)	002	15.84	
			4.5–4.6	br	<i>h</i> ₁		
2	SmA	78	32.91	VS (sh)	001	32.88	<i>d</i> = 32.88 Å <i>V</i> _{mol} ≈ 1098 Å ³ <i>A</i> _M ≈ 66.8 Å ² <i>σ</i> _{ch} ≈ 22.2 Å ²
			16.42	W (sh)	002	16.44	
			4.4–4.5	br	<i>h</i> ₁		

¹ The *d*_{obs.} and *d*_{calcd.} values refer to the measured and calculated diffraction spacings, respectively. *d*_{calcd.} = $\langle d_{001} \rangle = [\sum_l d_{00l} I] / N_{00l}$, in which *N*_{00l} = the number of (00l) reflections. ² *I* is the intensity of each reflection: VS = very strong, W = weak, sh = sharp reflection, and br = broad reflection. ³ *hkl* are the Miller indices of the reflections. *h*₁ indicates the center position of the diffuse wide-angle signal that originates from the lateral short-range order of the ionic moieties (c.f. *h*_{ion}) and the molten alkyl chains (c.f. *h*_{ch}). ⁴ *V*_{mol} is the molecular volume, which was estimated as *V*_{mol}(*T*) = (*M*_{cation}/0.6022)*f* + *V*_{iodide}, in which *M*_{cation} is the molecular mass of the cations (in g·mol^{−1}), *f* is a temperature-correcting factor (*f* = 0.9813 + 7.474 × 10^{−4}*T* with *T* in °C) and *V*_{iodide} is the partial volume of the iodide anions as determined from reference salts [61]. *A*_M is the cross-sectional area that is occupied by molecular assemblies along the sequence of smectic layers and was calculated as *A*_M(*T*) = 2*V*_{mol}(*T*)/*d*(*T*) [38,61]. The cross-sectional area of one fully stretched aliphatic chain, *σ*_{ch} [62], is listed for comparison.

From the structural parameters that were obtained from the SWAXS measurements as well as the temperature-dependent molecular volumes calculated for **1-15** and **2**, it can be concluded that the SmA phases are characterized by alternating, nanosegregated ionic and aliphatic sublayers, with a head-to-head arrangement of the ionic headgroups in the former, and partially interdigitated and folded alkyl chains in the latter [63,64]. The values calculated for the molecular cross-sectional areas, *A*_M (see Table 2), are comparable to those previously reported for the SmA phases adopted by

2-aryl-1,3-dimethylimidazolium iodide salts having two alkyl chains per cation (**6-*n*** (*n* = 6, 10, 14)) [38]. The supramolecular arrangements found in all of these SmA phases are similar. We note that **1-15** has been reported to spontaneously form thermodynamically stable vesicles in buffered aqueous media without the addition of other lipids [52]. As such, the structure of its thermotropic LC mesophase may resemble the local structure of the vesicle bilayer membranes. It was also found that **1-7** does not form bilayer vesicles under similar conditions [52]. Herein we report that it does not form a thermotropic LC mesophase either.

4. Discussion

The observation of SmA mesophases for imidazolium salts **1-*n*** (*n* = 11, 15) and **2** was not unexpected, since structurally related 1,3-bis(*n*-alkyl)imidazolium salts with long alkyl chains are known to adopt thermotropic SmA phases [54–59]. However, inspection of the literature data, some of which are collected in Table 3, shows that the clearing points of the 4,5-disubstituted ILCs are lower than those of 1,3-analogues. For example, the alkyl substituents of iodide salt **5-16** contain only one more methylene group than **1-15** or **2**, yet the clearing point of the former is 59 °C higher and its SmA phase is stable over a temperature range of 80 °C [54]. Even the homologue with *n*-dodecyl groups in the 1- and 3-positions, **5-12**, exhibits a similar clearing point as **1-15** and **2** despite its lower amphiphilic character. Since **5-12** also has a lower melting point, its mesophase temperature range is about 49 °C [56]. Likewise, [C₁₆C₁₆im][BF₄] and [C₁₆C₁₆im][PF₆] display higher clearing points and, thus, more stable SmA phases than **1-15** or **2** (we note that [BF₄][−] has a similar volume as the iodide anion, while [PF₆][−] is about 1.5 times as large [65]) [54,57]. Compound **1-11** also has a higher melting point and lower clearing point than **5-12** [56]. As such, 1,3-disubstitution appears to induce thermotropic LC mesomorphism in imidazolium salts more effectively than the 4,5-disubstituted analogues.

Table 3. A comparison of the thermal phase characteristics exhibited by 1,3-bis(*n*-alkyl)substituted imidazolium salts and the 4,5-bis(*n*-alkyl)imidazolium salts **1-11**, **1-15**, and **2**.

Compound ¹	Phase Transition Temperatures (°C) ²
1-7	Cr · 26 · Iso
1-11	HR1: Cr · ~55 ³ · SmA · 77 · Iso HR2: g · ~−14 · SmA · 76 · Iso
1-15	Cr · 76 · SmA · 88 · Iso
2	Cr · 70 · SmA · 88 · Iso
[C ₁₀ C ₁₀ im][I] (5-10) [54]	Cr · < 0 · SmA · 55 · Iso
[C ₁₂ C ₁₂ im][I] (5-12) [56]	Cr · 40 · SmA · 89 · Iso
[C ₁₆ C ₁₆ im][I] (5-16) [54]	Cr · 67 · SmA · 147 · Iso
[C ₁₀ C ₁₀ im][BF ₄] [57]	Cr · 18 · SmA · 25 · Iso
[C ₁₂ C ₁₂ im][BF ₄] [57]	Cr · 50 · SmA · 69 · Iso
[C ₁₄ C ₁₄ im][BF ₄] [57]	Cr · 63 · SmA · 106 · Iso
[C ₁₆ C ₁₆ im][BF ₄] [57]	Cr · 70 · SmA · 125 · Iso
[C ₁₀ C ₁₀ im][PF ₆] [54,66]	Cr · 16 · Iso
[C ₁₂ C ₁₂ im][PF ₆] [54,57]	Cr · 45 · Iso
[C ₁₄ C ₁₄ im][PF ₆] [54]	Cr · 59 · SmA · 81 · Iso
[C ₁₆ C ₁₆ im][PF ₆] [54]	Cr · 68 · SmA · 105 · Iso

¹ [C_{*n*}C_{*n*}im]⁺ = 1,3-bis(*n*-alkyl)imidazolium, where the subscript *n* indicates the number of carbon atoms in the alkyl chains. ² Abbreviations: Cr = crystalline phase; g = glass; SmA = smectic A phase; Iso = isotropic liquid phase. HR1 = first heating run; HR2 = second heating run. ³ See Table 1.

While the reasons underlying the aforementioned deduction are unclear, the imidazolium H(4) and H(5) atoms are known to participate in hydrogen bonds with halide counterions (see, for example, reference [67]), which may stabilize the ionic sublayers in the smectic mesophases. Replacement of the hydrogen atoms by long alkyl chains may impede such hydrogen-bond interactions. The steric parameters of the methyl groups in the 1- and 3-positions may also hinder compact arrangement of

the ionic headgroups in the ionic sublayers, although: (1) similar A_M values were found for the SmA phases adopted by 2-aryl-1,3-dimethylimidazolium iodide salts having two alkyl chains per cation (see above) and those smectic phases were stable until 147–164 °C [38], and (2) LC mesophases were not detected for thiazolium salt **3** which features only one *N*-methyl group. The latter observation provides another example of how subtle structural and electronic changes in organic salts may have a considerable impact on their physical properties. Although LC thiazolium salts have not yet been reported to the best of our knowledge, the apparent absence of mesomorphic properties for compound **3** does not exclude the possibility that 3-alkylthiazolium salts with relatively long alkyl chains may show such characteristics.

We tentatively ascribe the higher melting point of imidazoliums **1-11** and **1-15** as compared with **5-12** and **5-16**, respectively, to a closer proximity of the alkyl chains in the former. Such arrangement may facilitate van der Waals interactions between the chains and increase the melting point.

As mentioned above, a LC phase was not observed for **4**. The potential beneficial effect of the N–H sites in the cationic headgroup, which could participate in hydrogen bonds within ionic sublayers, may be counteracted by a mismatch in cross-sectional area between the ionic moieties and the molten, long alkyl chains, which is a prerequisite for the development of a smectic LC mesophase. The latter effect may explain the direct transition to an isotropic liquid and the lowest measured melting point among the series (**1-15**)–**4**.

We also note that **6-15** exhibits enantiotropic cubic and columnar LC mesophases while homologues with shorter alkyl chains adopt only SmA phases [38]. The absence of non-smectic LC phases for the salts discussed herein underscores the importance of the “taper angles” and precise geometric shapes of the polar headgroups of amphiphilic mesogens for inducing columnar and bicontinuous cubic mesophases [68–70].

5. Conclusions

We report the thermal properties for a series of 4,5-bis(*n*-alkyl)azolium salts. The majority of previously reported imidazolium- and thiazolium-based ionic liquids and ionic liquid crystals featured 1,3-disubstituted or *N*-substituted cations, respectively. The attachment of two long alkyl chains in the 4- and 5-positions of imidazolium or thiazolium rings is unusual because it requires a different synthetic approach than simply alkylating commercially available precursors, such as 1-methylimidazole, imidazole, or thiazole. While 1,3-dimethyl-4,5-bis(*n*-heptyl)imidazolium iodide (**1-7**) is non-mesomorphic, 1,3-dimethyl-4,5-bis(*n*-undecyl)imidazolium iodide (**1-11**), 1,3-dimethyl-4,5-bis(*n*-pentadecyl)imidazolium iodide (**1-15**) and the analogue with an additional methyl group in the 2-position (**2**) were found to be liquid-crystalline; they adopt SmA phases upon heating albeit over relatively narrow temperature ranges. For comparison, 3-methyl-4,5-bis(*n*-pentadecyl)thiazolium iodide (**3**) or 2-amino-4,5-bis(*n*-pentadecyl)imidazolium chloride (**4**) did not display liquid-crystalline properties under the conditions explored. Regardless, installing relatively long alkyl substituents in the 4- and 5-positions of the imidazolium salts appears to result in increased melting points and lowered clearing points, particularly when compared to data reported for 1,3-disubstituted analogues. The observation may be attributed to changes in hydrogen-bonding interactions, increased steric requirements of the ionic headgroups due to the *N*-methyl groups, and/or differences in proximity of the long alkyl chains. It remains to be seen whether non-smectic mesophases can be formed by 4,5-dialkylazolium salts. Further synthetic developments may be needed to answer these questions.

Supplementary Materials: The following are available online at <http://www.mdpi.com/2073-4352/9/1/34/s1>, Figures S1–S6: DSC data recorded for compounds **1-*n*** (*n* = 7, 11, 15) and **2-4**, Figure S7: TGA data recorded for compounds **1-15** and **2-4**, Figure S8: synchrotron-based SWAXS pattern that was recorded for compound **2** at 78 °C, Figure S9: synchrotron-based SWAXS patterns that were recorded for compound **3** at different temperatures.

Author Contributions: K.G. and F.G. conceived the project; C.W.B. supervised the project; L.R. synthesized compounds **1-*n*** (*n* = 7, 11, 15), **2**, and **3**; R.H. synthesized compound **4**; K.G. performed the thermal and structural characterizations (TGA, DSC, POM, synchrotron-based SWAXS) and analyzed the data; T.J.S. supervised the synchrotron-based SWAXS measurements; K.G. wrote the manuscript with contributions from all authors.

Funding: K.G. and C.W.B. were supported in part by the Institute for Basic Science (IBS-R019-D1). C.W.B. acknowledges the BK21 Plus Program as funded by the Ministry of Education and the National Research Foundation of Korea for support. L.R., R.H. and F.G. gratefully acknowledge the Deutsche Forschungsgemeinschaft (SFB 858). The experiments at the PLS-II 6D UNIST-PAL Synchrotron Beamline were supported in part by the Korean Ministry of Science and ICT (MSIT), Pohang University of Science and Technology (POSTECH) and the UNIST Central Research Facilities (UCRF).

Acknowledgments: We thank Seong-Hun Lee and Juhyun Yang for their assistance with the synchrotron measurements.

Conflicts of Interest: The authors declare no conflict of interest. The funders had no role in the design of the study; in the collection, analyses, or interpretation of data; in the writing of the manuscript, or in the decision to publish the results.

References

1. Bowlas, C.J.; Bruce, D.W.; Seddon, K.R. Liquid-Crystalline Ionic Liquids. *Chem. Commun.* **1996**, 1625–1626. [[CrossRef](#)]
2. Gordon, C.M.; Holbrey, J.D.; Kennedy, A.R.; Seddon, K.R. Ionic Liquid Crystals: Hexafluorophosphate Salts. *J. Mater. Chem.* **1998**, *8*, 2627–2636. [[CrossRef](#)]
3. Holbrey, J.D.; Seddon, K.R. The Phase Behaviour of 1-Alkyl-3-Methylimidazolium Tetrafluoroborates; Ionic Liquids and Ionic Liquid Crystals. *J. Chem. Soc. Dalton Trans.* **1999**, 2133–2139. [[CrossRef](#)]
4. Goossens, K.; Lava, K.; Nockemann, P.; Van Hecke, K.; Van Meervelt, L.; Driesen, K.; Görrler-Walrand, C.; Binnemans, K.; Cardinaels, T. Pyrrolidinium Ionic Liquid Crystals. *Chem. Eur. J.* **2009**, *15*, 656–674. [[CrossRef](#)] [[PubMed](#)]
5. Goossens, K.; Lava, K.; Bielawski, C.W.; Binnemans, K. Ionic Liquid Crystals: Versatile Materials. *Chem. Rev.* **2016**, *116*, 4643–4807. [[CrossRef](#)] [[PubMed](#)]
6. Mansueto, M.; Laschat, S. Ionic Liquid Crystals. In *Handbook of Liquid Crystals. Volume 6: Nanostructured and Amphiphilic Liquid Crystals*, 2nd ed.; Goodby, J.W., Collings, P.J., Kato, T., Tschierske, C., Gleeson, H., Raynes, P., Eds.; Wiley-VCH: Weinheim, Germany, 2014; pp. 231–280.
7. Fernandez, A.A.; Kouwer, P.H.J. Key Developments in Ionic Liquid Crystals. *Int. J. Mol. Sci.* **2016**, *17*, 731. [[CrossRef](#)] [[PubMed](#)]
8. Kato, T.; Yoshio, M.; Ichikawa, T.; Soberats, B.; Ohno, H.; Funahashi, M. Transport of Ions and Electrons in Nanostructured Liquid Crystals. *Nat. Rev. Mater.* **2017**, *2*, 17001. [[CrossRef](#)]
9. Kato, T.; Uchida, J.; Ichikawa, T.; Sakamoto, T. Functional Liquid Crystals towards the Next Generation of Materials. *Angew. Chem. Int. Ed.* **2018**, *57*, 4355–4371. [[CrossRef](#)]
10. Yamanaka, N.; Kawano, R.; Kubo, W.; Kitamura, T.; Wada, Y.; Watanabe, M.; Yanagida, S. Ionic Liquid Crystal as a Hole Transport Layer of Dye-Sensitized Solar Cells. *Chem. Commun.* **2005**, 740–742. [[CrossRef](#)]
11. Yamanaka, N.; Kawano, R.; Kubo, W.; Masaki, N.; Kitamura, T.; Wada, Y.; Watanabe, M.; Yanagida, S. Dye-Sensitized TiO₂ Solar Cells Using Imidazolium-Type Ionic Liquid Crystal Systems As Effective Electrolytes. *J. Phys. Chem. B* **2007**, *111*, 4763–4769. [[CrossRef](#)]
12. Högberg, D.; Soberats, B.; Yatagai, R.; Uchida, S.; Yoshio, M.; Kloo, L.; Segawa, H.; Kato, T. Liquid-Crystalline Dye-Sensitized Solar Cells: Design of Two-Dimensional Molecular Assemblies for Efficient Ion Transport and Thermal Stability. *Chem. Mater.* **2016**, *28*, 6493–6500. [[CrossRef](#)]
13. Bruce, D.W.; Gao, Y.A.; Canongia Lopes, J.N.; Shimizu, K.; Slattery, J.M. Liquid-Crystalline Ionic Liquids As Ordered Reaction Media for the Diels-Alder Reaction. *Chem. Eur. J.* **2016**, *22*, 16113–16123. [[CrossRef](#)] [[PubMed](#)]
14. Yazaki, S.; Funahashi, M.; Kato, T. An Electrochromic Nanostructured Liquid Crystal Consisting of π -Conjugated and Ionic Moieties. *J. Am. Chem. Soc.* **2008**, *130*, 13206–13207. [[CrossRef](#)] [[PubMed](#)]
15. Yazaki, S.; Funahashi, M.; Kagimoto, J.; Ohno, H.; Kato, T. Nanostructured Liquid Crystals Combining Ionic and Electronic Functions. *J. Am. Chem. Soc.* **2010**, *132*, 7702–7708. [[CrossRef](#)] [[PubMed](#)]
16. Beneduci, A.; Cospito, S.; La Deda, M.; Veltri, L.; Chidichimo, G. Electrofluorochromism in π -Conjugated Ionic Liquid Crystals. *Nat. Commun.* **2014**, *5*, 3105. [[CrossRef](#)] [[PubMed](#)]
17. Hayes, R.; Warr, G.G.; Atkin, R. Structure and Nanostructure in Ionic Liquids. *Chem. Rev.* **2015**, *115*, 6357–6426. [[CrossRef](#)] [[PubMed](#)]

18. Ji, Y.; Shi, R.; Wang, Y.; Saielli, G. Effect of the Chain Length on the Structure of Ionic Liquids: From Spatial Heterogeneity to Ionic Liquid Crystals. *J. Phys. Chem. B* **2013**, *117*, 1104–1109. [[CrossRef](#)]
19. Nemoto, F.; Kofu, M.; Yamamuro, O. Thermal and Structural Studies of Imidazolium-Based Ionic Liquids with and Without Liquid-Crystalline Phases: The Origin of Nanostructure. *J. Phys. Chem. B* **2015**, *119*, 5028–5034. [[CrossRef](#)]
20. Russina, O.; Lo Celso, F.; Plechkova, N.; Jafta, C.J.; Appetecchi, G.B.; Triolo, A. Mesoscopic Organization in Ionic Liquids. *Top. Curr. Chem.* **2017**, *375*, 58. [[CrossRef](#)]
21. Russina, O.; Lo Celso, F.; Plechkova, N.V.; Triolo, A. Emerging Evidences of Mesoscopic-Scale Complexity in Neat Ionic Liquids and Their Mixtures. *J. Phys. Chem. Lett.* **2017**, *8*, 1197–1204. [[CrossRef](#)]
22. Bruce, D.W.; Cabry, C.P.; Canongia Lopes, J.N.; Costen, M.L.; D’Andrea, L.; Grillo, I.; Marshall, B.C.; McKendrick, K.G.; Minton, T.K.; Purcell, S.M.; et al. Nanosegregation and Structuring in the Bulk and at the Surface of Ionic-Liquid Mixtures. *J. Phys. Chem. B* **2017**, *121*, 6002–6020. [[CrossRef](#)] [[PubMed](#)]
23. Pontoni, D.; Haddad, J.; Di Michiel, M.; Deutsch, M. Self-Segregated Nanostructure in Room Temperature Ionic Liquids. *Soft Matter* **2017**, *13*, 6947–6955. [[CrossRef](#)]
24. Cosby, T.; Vicars, Z.; Wang, Y.; Sangoro, J. Dynamic-Mechanical and Dielectric Evidence of Long-Lived Mesoscale Organization in Ionic Liquids. *J. Phys. Chem. Lett.* **2017**, *8*, 3544–3548. [[CrossRef](#)] [[PubMed](#)]
25. Nemoto, F.; Kofu, M.; Nagao, M.; Ohishi, K.; Takata, S.; Suzuki, J.; Yamada, T.; Shibata, K.; Ueki, T.; Kitazawa, Y.; et al. Neutron Scattering Studies on Short- and Long-Range Layer Structures and Related Dynamics in Imidazolium-Based Ionic Liquids. *J. Chem. Phys.* **2018**, *149*, 054502. [[CrossRef](#)] [[PubMed](#)]
26. Cabry, C.P.; D’Andrea, L.; Shimizu, K.; Grillo, I.; Li, P.; Rogers, S.; Bruce, D.W.; Canongia Lopes, J.N.; Slattery, J.M. Exploring the Bulk-Phase Structure of Ionic Liquid Mixtures Using Small-Angle Neutron Scattering. *Faraday Discuss.* **2018**, *206*, 265–289. [[CrossRef](#)] [[PubMed](#)]
27. Cao, W.D.; Wang, Y.T.; Saielli, G. Metastable State During Melting and Solid-Solid Phase Transition of $[C_n\text{Mim}][\text{NO}_3]$ ($n = 4\text{--}12$) Ionic Liquids by Molecular Dynamics Simulation. *J. Phys. Chem. B* **2018**, *122*, 229–239. [[CrossRef](#)] [[PubMed](#)]
28. Douce, L.; Suisse, J.-M.; Guillon, D.; Taubert, A. Imidazolium-Based Liquid Crystals: A Modular Platform for Versatile New Materials with Finely Tuneable Properties and Behaviour. *Liq. Cryst.* **2011**, *38*, 1653–1661. [[CrossRef](#)]
29. Bara, J.E.; Shannon, M.S. Beyond 1,3-Difunctionalized Imidazolium Cations. *Nanomater. Energy* **2012**, *1*, 237–242. [[CrossRef](#)]
30. Scafani, V.F.; Alshaikh, A.A.; Bara, J.E. Analysis of the Frequency and Diversity of 1,3-Dialkylimidazolium Ionic Liquids Appearing in the Literature. *Ind. Eng. Chem. Res.* **2018**, *57*, 15971–15981. [[CrossRef](#)]
31. Fox, D.M.; Awad, W.H.; Gilman, J.W.; Maupin, P.H.; De Long, H.C.; Trulove, P.C. Flammability, Thermal Stability, and Phase Change Characteristics of Several Trialkylimidazolium Salts. *Green Chem.* **2003**, *5*, 724–727. [[CrossRef](#)]
32. Mukai, T.; Yoshio, M.; Kato, T.; Ohno, H. Effect of Methyl Groups Onto Imidazolium Cation Ring on Liquid Crystallinity and Ionic Conductivity of Amphiphilic Ionic Liquids. *Chem. Lett.* **2004**, *33*, 1630–1631. [[CrossRef](#)]
33. Mukai, T.; Yoshio, M.; Kato, T.; Yoshizawa-Fujita, M.; Ohno, H. Self-Organization of Protonated 2-Heptadecylimidazole as an Effective Ion Conductive Matrix. *Electrochemistry* **2005**, *73*, 623–626.
34. Kouwer, P.H.J.; Swager, T.M. Synthesis and Mesomorphic Properties of Rigid-Core Ionic Liquid Crystals. *J. Am. Chem. Soc.* **2007**, *129*, 14042–14052. [[CrossRef](#)] [[PubMed](#)]
35. Yoshio, M.; Ichikawa, T.; Shimura, H.; Kagata, T.; Hamasaki, A.; Mukai, T.; Ohno, H.; Kato, T. Columnar Liquid-Crystalline Imidazolium Salts. Effects of Anions and Cations on Mesomorphic Properties and Ionic Conductivity. *Bull. Chem. Soc. Jpn.* **2007**, *80*, 1836–1841. [[CrossRef](#)]
36. Alam, M.A.; Motoyanagi, J.; Yamamoto, Y.; Fukushima, T.; Kim, J.; Kato, K.; Takata, M.; Saeki, A.; Seki, S.; Tagawa, S.; et al. “Bicontinuous Cubic” Liquid Crystalline Materials from Discotic Molecules: A Special Effect of Paraffinic Side Chains with Ionic Liquid Pendants. *J. Am. Chem. Soc.* **2009**, *131*, 17722–17723. [[CrossRef](#)] [[PubMed](#)]
37. Li, C.H.; He, J.H.; Liu, J.H.; Qian, L.A.; Yu, Z.Q.; Zhang, Q.L.; He, C.X. Liquid Crystalline Phases of 1,2-Dimethyl-3-Hexadecylimidazolium Bromide and Binary Mixtures With Water. *J. Colloid Interface Sci.* **2010**, *349*, 224–229. [[CrossRef](#)]

38. Goossens, K.; Wellens, S.; Van Hecke, K.; Van Meervelt, L.; Cardinaels, T.; Binnemans, K. T-Shaped Ionic Liquid Crystals Based on the Imidazolium Motif: Exploring Substitution of the C-2 Imidazolium Carbon Atom. *Chem. Eur. J.* **2011**, *17*, 4291–4306. [[CrossRef](#)]
39. Fernandez, A.A.; de Haan, L.T.; Kouwer, P.H.J. Towards Room-Temperature Ionic Liquid Crystals. *J. Mater. Chem. A* **2013**, *1*, 354–357. [[CrossRef](#)]
40. Nestor, S.T.; Heinrich, B.; Sykora, R.A.; Zhang, X.; McManus, G.J.; Douce, L.; Mirjafari, A. Methimazolium-Based Ionic Liquid Crystals: Emergence of Mesomorphic Properties via a Sulfur Motif. *Tetrahedron* **2017**, *73*, 5456–5460. [[CrossRef](#)]
41. Hindman, M.S.; Stanton, A.D.; Christopher Irvin, A.; Wallace, D.A.; Moon, J.D.; Reclusado, K.R.; Liu, H.; Belmore, K.A.; Liang, Q.; Shannon, M.S.; et al. Synthesis of 1,2-Dialkyl-, 1,4(5)-Dialkyl-, and 1,2,4(5)-Trialkylimidazoles via a One-Pot Method. *Ind. Eng. Chem. Res.* **2013**, *52*, 11880–11887. [[CrossRef](#)]
42. Yue, S.; Roveda, J.D.; Mittenthal, M.S.; Shannon, M.S.; Bara, J.E. Experimental Densities and Calculated Fractional Free Volumes of Ionic Liquids With Tri- and Tetra-Substituted Imidazolium Cations. *J. Chem. Eng. Data* **2018**, *63*, 2522–2532. [[CrossRef](#)]
43. Fumino, K.; Wulf, A.; Ludwig, R. Strong, Localized, and Directional Hydrogen Bonds Fluidize Ionic Liquids. *Angew. Chem. Int. Ed.* **2008**, *47*, 8731–8734. [[CrossRef](#)] [[PubMed](#)]
44. Fumino, K.; Wulf, A.; Ludwig, R. The Potential Role of Hydrogen Bonding in Aprotic and Protic Ionic Liquids. *Phys. Chem. Chem. Phys.* **2009**, *11*, 8790–8794. [[CrossRef](#)] [[PubMed](#)]
45. Roth, C.; Peppel, T.; Fumino, K.; Köckerling, M.; Ludwig, R. The Importance of Hydrogen Bonds for the Structure of Ionic Liquids: Single-Crystal X-ray Diffraction and Transmission and Attenuated Total Reflection Spectroscopy in the Terahertz Region. *Angew. Chem. Int. Ed.* **2010**, *49*, 10221–10224. [[CrossRef](#)] [[PubMed](#)]
46. Wulf, A.; Fumino, K.; Ludwig, R. Spectroscopic Evidence for an Enhanced Anion-Cation Interaction from Hydrogen Bonding in Pure Imidazolium Ionic Liquids. *Angew. Chem. Int. Ed.* **2010**, *49*, 449–453. [[CrossRef](#)] [[PubMed](#)]
47. Peppel, T.; Roth, C.; Fumino, K.; Paschek, D.; Köckerling, M.; Ludwig, R. The Influence of Hydrogen-Bond Defects on the Properties of Ionic Liquids. *Angew. Chem. Int. Ed.* **2011**, *50*, 6661–6665. [[CrossRef](#)] [[PubMed](#)]
48. Fumino, K.; Peppel, T.; Geppert-Rybczynska, M.; Zaitsau, D.H.; Lehmann, J.K.; Verevkin, S.P.; Köckerling, M.; Ludwig, R. The Influence of Hydrogen Bonding on the Physical Properties of Ionic Liquids. *Phys. Chem. Chem. Phys.* **2011**, *13*, 14064–14075. [[CrossRef](#)]
49. Hugar, K.M.; Kostalik, H.A.; Coates, G.W. Imidazolium Cations with Exceptional Alkaline Stability: A Systematic Study of Structure-Stability Relationships. *J. Am. Chem. Soc.* **2015**, *137*, 8730–8737. [[CrossRef](#)]
50. Wang, D.; Richter, C.; Rühling, A.; Drücker, P.; Siegmund, D.; Metzler-Nolte, N.; Glorius, F.; Galla, H.-J. A Remarkably Simple Class of Imidazolium-Based Lipids and Their Biological Properties. *Chem. Eur. J.* **2015**, *21*, 15123–15126. [[CrossRef](#)]
51. Rühling, A.; Wang, D.; Ernst, J.B.; Wulff, S.; Honeker, R.; Richter, C.; Ferry, A.; Galla, H.-J.; Glorius, F. Influence of the Headgroup of Azolium-Based Lipids on Their Biophysical Properties and Cytotoxicity. *Chem. Eur. J.* **2017**, *23*, 5920–5924. [[CrossRef](#)]
52. Drücker, P.; Rühling, A.; Grill, D.; Wang, D.; Draeger, A.; Gerke, V.; Glorius, F.; Galla, H.-J. Imidazolium Salts Mimicking the Structure of Natural Lipids Exploit Remarkable Properties Forming Lamellar Phases and Giant Vesicles. *Langmuir* **2017**, *33*, 1333–1342. [[CrossRef](#)] [[PubMed](#)]
53. Rakers, L.; Glorius, F. Flexible Design of Ionic Liquids for Membrane Interactions. *Biophys. Rev.* **2018**, *10*, 747–750. [[CrossRef](#)] [[PubMed](#)]
54. Rondla, R.; Lee, C.K.; Lu, J.T.; Lin, I.J.B. Symmetrical 1,3-Dialkylimidazolium Based Ionic Liquid Crystals. *J. Chin. Chem. Soc.* **2013**, *60*, 745–754.
55. Wang, X.; Heinemann, F.W.; Yang, M.; Melcher, B.U.; Fekete, M.; Mudring, A.-V.; Wasserscheid, P.; Meyer, K. A New Class of Double Alkyl-Substituted, Liquid Crystalline Imidazolium Ionic Liquids—A Unique Combination of Structural Features, Viscosity Effects, and Thermal Properties. *Chem. Commun.* **2009**, 7405–7407. [[CrossRef](#)] [[PubMed](#)]
56. Wang, X.; Vogel, C.S.; Heinemann, F.W.; Wasserscheid, P.; Meyer, K. Solid-State Structures of Double-Long-Chain Imidazolium Ionic Liquids: Influence of Anion Shape on Cation Geometry and Crystal Packing. *Cryst. Growth Des.* **2011**, *11*, 1974–1988. [[CrossRef](#)]

57. Wang, X.; Sternberg, M.; Kohler, F.T.U.; Melcher, B.U.; Wasserscheid, P.; Meyer, K. Long-Alkyl-Chain-Derivatized Imidazolium Salts and Ionic Liquid Crystals with Tailor-Made Properties. *RSC Adv.* **2014**, *4*, 12476–12481. [[CrossRef](#)]
58. Yang, M.; Mallick, B.; Mudring, A.-V. A Systematic Study on the Mesomorphic Behavior of Asymmetrical 1-Alkyl-3-Dodecylimidazolium Bromides. *Cryst. Growth Des.* **2014**, *14*, 1561–1571. [[CrossRef](#)]
59. Lee, C.K.; Peng, H.H.; Lin, I.J.B. Liquid Crystals of *N,N'*-Dialkylimidazolium Salts Comprising Palladium(II) and Copper(II) Ions. *Chem. Mater.* **2004**, *16*, 530–536. [[CrossRef](#)]
60. Ngo, H.L.; LeCompte, K.; Hargens, L.; McEwen, A.B. Thermal Properties of Imidazolium Ionic Liquids. *Thermochim. Acta* **2000**, *357*, 97–102. [[CrossRef](#)]
61. Park, G.; Goossens, K.; Shin, T.J.; Bielawski, C.W. Dicyanamide Salts That Adopt Smectic, Columnar, or Bicontinuous Cubic Liquid-Crystalline Mesophases. *Chem. Eur. J.* **2018**, *24*, 6399–6411. [[CrossRef](#)]
62. Marcos, M.; Giménez, R.; Serrano, J.L.; Donnio, B.; Heinrich, B.; Guillon, D. Dendromesogens: Liquid Crystal Organizations of Poly(Amidoamine) Dendrimers Versus Starburst Structures. *Chem. Eur. J.* **2001**, *7*, 1006–1013. [[CrossRef](#)]
63. Fouchet, J.; Douce, L.; Heinrich, B.; Welter, R.; Louati, A. A Convenient Method for Preparing Rigid-Core Ionic Liquid Crystals. *Beilstein J. Org. Chem.* **2009**, *5*, No. 51. [[CrossRef](#)] [[PubMed](#)]
64. Dobbs, W.; Douce, L.; Heinrich, B. 1-(4-Alkyloxybenzyl)-3-methyl-1*H*-imidazol-3-ium Organic Backbone: A Versatile Smectogenic Moiety. *Beilstein J. Org. Chem.* **2009**, *5*, No. 62. [[CrossRef](#)] [[PubMed](#)]
65. Jenkins, H.D.B.; Roobottom, H.K.; Passmore, J.; Glasser, L. Relationships among Ionic Lattice Energies, Molecular (Formula Unit) Volumes, and Thermochemical Radii. *Inorg. Chem.* **1999**, *38*, 3609–3620. [[CrossRef](#)] [[PubMed](#)]
66. Dzyuba, S.V.; Bartsch, R.A. New Room-Temperature Ionic Liquids with C_2 -Symmetrical Imidazolium Cations. *Chem. Commun.* **2001**, *16*, 1466–1467. [[CrossRef](#)]
67. Goossens, K.; Nockemann, P.; Driesen, K.; Goderis, B.; Görrler-Walrand, C.; Van Hecke, K.; Van Meervelt, L.; Pouzet, E.; Binnemans, K.; Cardinaels, T. Imidazolium Ionic Liquid Crystals With Pendant Mesogenic Groups. *Chem. Mater.* **2008**, *20*, 157–168. [[CrossRef](#)]
68. Tschierske, C. Liquid Crystal Engineering—New Complex Mesophase Structures and Their Relations to Polymer Morphologies, Nanoscale Patterning and Crystal Engineering. *Chem. Soc. Rev.* **2007**, *36*, 1930–1970. [[CrossRef](#)] [[PubMed](#)]
69. Ichikawa, T.; Yoshio, M.; Hamasaki, A.; Taguchi, S.; Liu, F.; Zeng, X.; Ungar, G.; Ohno, H.; Kato, T. Induction of Thermotropic Bicontinuous Cubic Phases in Liquid-Crystalline Ammonium and Phosphonium Salts. *J. Am. Chem. Soc.* **2012**, *134*, 2634–2643. [[CrossRef](#)] [[PubMed](#)]
70. Ungar, G.; Liu, F.; Zeng, X. Cubic and Other 3D Thermotropic Liquid Crystal Phases and Quasicrystals. In *Handbook of Liquid Crystals. Volume 5: Non-Conventional Liquid Crystals*, 2nd ed.; Goodby, J.W., Collings, P.J., Kato, T., Tschierske, C., Gleeson, H., Raynes, P., Eds.; Wiley-VCH: Weinheim, Germany, 2014; pp. 363–436.

